A Mixed Epistemic-Aleatory Stochastic Framework for the Optimal Operation of Hybrid Fuel Stations

Behdad Faridpak, Meisam Farrokhifar, *Senior Member, IEEE*, Arman Alahyari and Mousa Marzband, *Senior Member, IEEE*

***Abstract*—The fast development of technologies in the smart grids provides new opportunities such as co-optimization of multi-energy systems. One of the new concepts that can utilize multiple energy sources is a hybrid fuel station (HFS). For instance, an HFS can benefit from energy hubs, renewable energies, and natural gas sources to supply electric vehicles along with natural gas vehicles. However, the optimal operation of an HFS deals with uncertainties from different sources that do not have similar natures. Some may lack in term of historical data, and some may have very random and unpredictable behavior. In this study, we present a stochastic mathematical framework to address both types of these uncertainties according to the innate nature of each uncertain variable, namely: epistemic uncertainty variables (EUVs) and aleatory uncertainty variables (AUVs). Also, the imprecise probability approach is introduced for EUVs utilizing the copula theory in the process, and a scenario-based approach combining Monte Carlo simulation with Latin Hypercube sampling is applied for AUVs. The proposed framework is employed to address the daily operation of a novel HFS, leading to a two-stage mixed-integer linear programming problem. The proposed approach and its applicability are verified using various numerical simulations.**

***Index Terms*—Hybrid fuel station, uncertainty, stochastic scheduling, imprecise probability.**

I. Introduction

In the last few years, the emergence of new technologies brought forward many challenges and opportunities within the concept of the smart grid. The trend is changing from managing and scheduling energy systems independently toward multi-energy systems integrating energy infrastructures with various natures such as natural gas and electricity [1]. Energy sources, as well as their networks and carriers, would ideally interact together continuously acquiring an appropriate management tool to combine operations of all system components [2]. In this regard, energy hub (EH) is introduced as an encouraging option to combine the management of multi-energy systems.

A. Motivation and Literature Review

EH employs various types of energy sources, converters and storages thus attracting many researches investigating the optimal operation of EHs [3]–[10]. In study [3], a multi-objective particle swarm optimization (MOPSO) method is utilized for optimizing EH performance. The optimal coupling of energy systems is addressed in [4], [5] utilizing a mixed-integer linear programming (MILP) approach. However, considering the structure of the optimization, other approaches such as alternating direction method of multipliers (ADMM) [6], multi-agent genetic algorithm (MAGA) [7] and a decomposed energy flow [8] were adopted to analyses the optimal operation of EHs. In this scope, other solutions also have been included, like stochastic dynamic programming (SDP) [9] and chance-constrained programming (CCP) [10].

EHs have several practical applications, one of which is in hybrid fuel stations (HFS) where, for instance, an electric vehicle (EV) can be supplied along with other types like a natural gas vehicle (NGV). In this sort of application, efficient charging of EVs and refueling of NGVs is a new challenge in the integrated management of EHs. Also, a structure to efficiently utilize EH source while charging vehicles in the station is required. There are studies that address the aforementioned issues but only separately. For example, in [11], the uncertain charging pattern of plug-in vehicles owners was modeled by a stochastic approach. The effect of price-based and incentive-based demand response programs (DRPs) on the optimal behavior of EV owners was proposed in [12]. The main stakeholders of EVs charging and NGVs refueling scheduling are the operators of HFS and vehicle owners. In this regard, a bi-objective optimization problem was formulated to optimize these stakeholders in [13] jointly. Furthermore, to reduce operation cost, the authors in [14] proposed an EV charging station integrated with energy storage (ES) and photovoltaic system (PV). For a compressed natural gas (CNG) station, the optimal switching process of the gas compressor (GC) was achieved considering electricity tariff in [15].

Note that, considering multi-energy systems that consist of an EH, in practical applications, the optimized operation faces various uncertainties that complexify the decision-making problem. The uncertainty sources in the previous researches

Manuscript received June 9, 2020; revised January 16, 2021, June 3, 2021; accepted August 1, 2021.

B. Faridpak is with the Faculty of Electrical and Computer Engineering, University of Tabriz, Tabriz 5166616471, Iran (e-mail: b.faridpak93@ms.tabrizu.ac.ir).

M. Farrokhifar (*Corresponding author*) is with the Center for Energy Science and Technology, Skoltech, Moscow 121205, Russia (e-mail: m.farrokhi@skoltech.ru).

A. Alahyari is with the Department of Electrical Engineering, Sharif University of Technology, Tehran 11155-11365, Iran (e-mail: alahyari_arman@ee.sharif.edu).

M. Marzband is with Faculty of Engineering and Environment, Northumbria University, Newcastle upon Tyne NE1 8ST, UK. (email: mousa.marzbandnorthumbria.ac.uk) and with the center of research excellence in renewable energy and power systems, King Abdulaziz University, Jeddah 21589, Saudi Arabia.

mostly include renewable generations, market prices and demand. There are several approaches available while dealing with uncertainty. The authors in [16] propose a probability density function (PDF)-based method combined with Latin Hypercube sampling (LHS) to address the uncertainty of renewable power generation. Other uncertainty approaches like the interval optimization method and point estimate method (PEM) to consider the uncertainty of generated power from wind with variable speed (υ) in wind turbines (WTs) as well as produced power from solar radiation (SR) in PVs were also investigated in recent studies [1], [17], [18]. Besides, Monte Carlo is also widely used when the generation of scenarios for uncertain parameters is required [19], [20]. However, uncertainty has more than one *dimension* or more generally more than one type depending on the nature of the uncertainty sources not adequately addressed in the related literature. In this regard, in terms of nature, the uncertainty variables can be classified into two different categories, including aleatory uncertainty variables (AUVs) and epistemic uncertainty variables (EUVs). According to their random laws, the AUVs sampling results from empirical distribution functions and statistical estimates of the probabilities. In contrast, EUVs include uncertainty variables with lack-of-knowledge about formulations, parameters, and input data [21].

B. Proposed Approach and Paper Contributions

In this study, at first, we introduce different aspects of uncertainty quantification and how to differentiate between uncertainties. We present a general mathematical approach incorporating aleatory variability and epistemic uncertainty features applicable in cases that a decision-maker faces multiple uncertainties. In practical applications, all uncertainties should not be modeled with the same approach. For instance, conventional approaches, such as scenario-based approaches are not practical to address uncertainties that lack a proper set of historical data. Besides, in the scenario-based approaches [5], [16], [20], [23], the scenarios with a high probability of occurrences are selected, mostly neglecting extreme and infrequent situations. To address this issue, it is possible to increase the number of scenarios with the side effect of the complexity and extra computational burden. Then, we introduce a framework for an HFS that supplies electric and gaseous vehicles. As the operator of this HFS deals with multiple uncertainties, generally with different natures, we apply the introduced mathematical approach for the optimal scheduling of HFS while counting for natures of multiple uncertainties. Finally, in the numerical studies with real-world data, we demonstrate the application of our approach in the proposed HFS daily operation.

Table I classifies proposed methodologies in EHs modeling and scheduling in terms of components, application, uncertainty handling and solution method. Accordingly, the contributions of the study are summarized as follows:

- Proposing a stochastic mathematical framework to include different quantifications of uncertainty variables in the optimization, namely: a mixed epistemic-aleatory uncertainty modeling framework.
- Providing a detailed HFS structure to supply two different types of vehicles while utilizing an EH.
- Incorporating the mixed uncertainty variable modeling in a two-stage probabilistic optimization model for the daily operation of the proposed HFS.

The remainder of the paper is organized as follows. Section II presents mathematical modeling of the uncertainty variables, scenario reduction, and HFS. Optimization framework of the proposed HFS is explained in Section III. Numerical results are illustrated in Section IV. Finally, Section V concludes the paper.

II. Mathematical Modelling

In this section, we first address the uncertainty quantification details and then present our uncertainty models within the introduced frameworks. Then, HFS and its components are introduced. Finally, mathematical approaches for the optimal daily operation of the HFS are demonstrated.

A. Uncertainty Variables Modeling

We propose an uncertainty modeling approach for an optimization where the decision-maker is dealing with multiple sources of uncertainties with different innate natures. In general, the uncertainty can have different conceptions and can be divided into two types [21], namely: EUVs, which are caused by the lack of information and in our study, we represent them by imprecise probabilities, and AUVs which are caused by the natural variability of random phenomena and we model them by a probability-based approach. Note that, the EUVs and AUVs are denoted by X and Y within this study, respectively. We explain the detail of each uncertainty type modeling in the next two subsections. This consideration is the main contribution of the paper in terms of uncertainty modeling. For instance, for the uncertainty variables such as EVs' load (L_{ev}) the lack of information raises uncertainties in state of charge (SOC), dwell times, demand distribution, driver preferences regarding charging and the market penetration of EVs. Therefore, we apply the imprecise probability to exhibit how explicit the precision of HFSs charging limitation is known. While, in practice, the implementation of conventional PDF-based approaches for this type of uncertainty variables is not efficient because the precise values of the model parameters might not be accurately estimated due to lack of data in the actual operational conditions. As a summary, we use this classification for uncertainty variables, since epistemic uncertainty is a severe problem for real-world operation. To better clarify the explained approaches, the overall process of uncertainty modeling for both types is demonstrated in a flowchart in Fig. 1.

1) Epistemic Uncertainty Variables Modeling: We apply imprecise probability to exhibit how explicit the precision of something is known. Indeed, the fundamental source of imprecision is incomplete knowledge of input variables. There is no exact rule to assume a specific probability for uncertain variables. They could realize to a random value within a random uncertainty set. The idea is to model the imprecision by considering a small random space between bounds when

TABLE I
THE COMPARISON OF DIFFERENT METHODS FOR EH OPTIMAL OPERATION

Reference	Components	Utilization	Uncertainty			Modeling method
			variables	characterization	modeling	
[1]	WT, PV, ES, C[1], P2G[2], GT[3], GS[4], GC	HFS	SR, υ, EV, NGV	Probability	2m+1PEM	MILP
[3]	WT, C, T[5], CHP[6], F[7]	Distribution system	EV, υ, price	Probability	2PEM	MOPSO
[4]	ES, T, CHP, TS[8], F	Distribution system	-	-	-	MILP
[5]	PV, WT, CHP, HP	Residential	SR	Probability	2PEM	MILP
[6]	PV, ES, SC[9], CHP, TS, HP[10], AC[11]	Residential	-	-	-	ADMM
[7]	T, CHP, F, HE[12]	Distribution system	-	-	-	MAGA
[8]	WT, PV, T, CHP, B[13]	Power system	SR, υ, load	Probability	2m+1PEM	Decomposed
[9]	ES, El, HS[14], FC[15], CHP, B, TS	Power system	Price, load	Probability	PDF	SDP
[10]	C, HP, F, CHP, WS[16]	Distribution system	SR, υ	Probability	PDF	CCP
[11]	WT, ES, CHP, TS, B	Parking lot	EV, υ	Probability	PDF	-
[22]	PV, HP, T, CHP, B, TS, ES, AR[17], AC	Residential	SR, load	Probability	PDF	MILP
Proposed	WT, PV, ES, C, P2G, GT, GS, GC	HFS	EV, NGV	Non-probability	Imprecise probability	Two-stage
			SR, υ, price	Probability	PDF	

[1]Converter, [2]Power to gas, [3]Gas turbine, [4]Gas storage, [5]Transformer, [6]Combined heat and power, [7]Furnace, [8]Thermal storage, [9]Solar combisystem, [10]Heating pump, [11]Absorption chiller, [12]Heat exchanger, [13]Boiler, [14]Hydrogen storage, [15]Fuel cell, [16]Water storage, [17]Air conditioner.

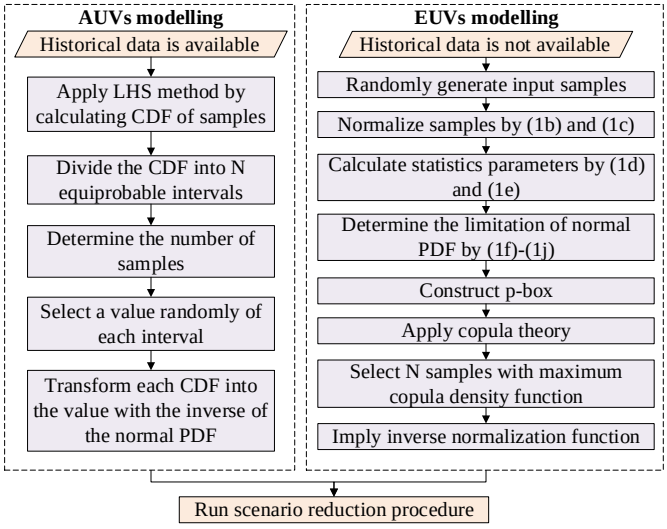

Fig. 1. Uncertainty variables modeling for each time period t.

SET 1 Mathematical model of stochastic framework

$$\square X = \left\{F(x) : \forall x \in \mathbb{R},\ \underline{F}(x) \le F(x) \le \overline{F}(x)\right\} \quad (1a)$$

$$Norm^{(1)}_{X,i+1} = \frac{x_{i+1} - x_i}{x_i} \qquad i \in \{0, 1, ..., N-1\} \quad (1b)$$

$$Norm^{(2)}_{X} = \frac{n}{N} \qquad n \in \{1, 2, ..., N\} \quad (1c)$$

$$\mu = \frac{1}{N}\sum\nolimits_{n=1}^{N} Norm^{(2)}_{X} \qquad \mu \in [0, 1] \quad (1d)$$

$$\sigma^2 = \frac{1}{N-1}\sum\nolimits_{n=1}^{N}\left(Norm^{(2)}_{X} - \mu\right)^2 \qquad \sigma \in (0, 1] \quad (1e)$$

$$f(x) = \frac{1}{\sqrt{2\pi\sigma^2}} e^{-\frac{(x-\mu)^2}{\sigma^2}} \quad (1f)$$

$$\left[\underline{\mu}, \overline{\mu}\right] = \left[\mu - z_{\alpha/2}\,\sigma/\sqrt{N}, \mu + z_{\alpha/2}\,\sigma/\sqrt{N}\right] \quad (1g)$$

$$z_{\alpha/2} = \Phi^{-1}(\alpha/2) \qquad \in [0, 1] \quad (1h)$$

$$\left[\underline{\sigma}^2, \overline{\sigma}^2\right] = \left[\sigma^2 - z_{\alpha/2}\,a, \sigma^2 + z_{\alpha/2}\,a\right] \quad (1i)$$

$$a = \sqrt{\left((N-1)^3/N^4\right)} \quad (1j)$$

enough previously known data is available (e.g., historical data), or a larger space when there is a lack of information regarding the epistemic uncertainty. The proposed stochastic framework regarding the epistemic uncertainty is demonstrated in (1). Indeed, imprecise probabilities for each real-valued, continuous and uncertain variable $X \in \{X_1, X_2, ..., X_{\tau 1}\}$ are the lower and upper cumulative distribution functions (CDFs) indicated by $\overline{F}(x)$ and $\underline{F}(x)$, respectively. These are the upper and lower probabilities of the X valued by $x \in \mathbb{R}$. This is the interpretation of probability bounds analysis visualized by the probability box (p-box) as demonstrated in (1a). Where $\square X$ denotes the p-box of X.

Indeed, the realizations of uncertain variable X, whose distribution function is unknown, are restricted within the p-box. When there is no extra data about the moments or distribution family more than what is implied by the two bounding CDFs. In this regard, the p-box representation of X can be denoted more compactly as $\left[\underline{F}(x), \overline{F}(x)\right]$ in which $\underline{F}(x), \overline{F}(x) : \mathbb{R} \to [0, 1]$. Alternatively, p-boxes could have a wider range of applications to deal with uncertainties compared to other similar probability theories such as interval probabilities [17], [18].

The imprecise probability modeling starts with generating, random samples $[x]^{N \times \tau_1}$ by Monte Carlo simulation in the range of X limitations $\left[\underline{X}, \overline{X}\right]$ as the input vector. Due to the dissimilar properties of uncertainty variables, the input data are normalized by defining a two-step normalization function for each X. At first step, all quantities of x in which $x : \mathbb{R} \to \left[\underline{X}, \overline{X}\right]$ are transformed into the $Norm^{(1)}_{X,i+1} : \mathbb{R} \to [-1, 1]$ by (1b). In the next step, to calculate the normalized data-sets of the second step, $Norm^{(2)}_{X} : \mathbb{R} \to [0, 1]$, we sort the data-sets numbered by n from first step to replace the smallest number with the value $1/N$, the second smallest normalization number with $2/N$ and so on until the largest number is replaced with the value $(N-1)/N$. This provides one ordering of numbers for each X as stated in (1c).

To derive p-box schematic of these samples, the normal distributions $\mathcal{N}\left(\mu, \sigma^2\right)$ with mean μ and standard deviation σ are obtained for each X from unbiased point estimates in (1d) and (1e). Considering the previous steps procedures, the

density function, $f(x)$, can also be obtained as shown in (1f). The p-box is defined based on unknown information about bivariate μ and σ^2. Note that, we presume the ranges of $[\underline{\mu}, \overline{\mu}]$ and $[\underline{\sigma}^2, \overline{\sigma}^2]$ for generated samples. The values of this marginal data are calculated by (1g)-(1j). Where, α determines the confidence level as $100(1-\alpha)\%$. As well, $z_{\alpha/2}$ is related to inverse standard normal $\Phi^{-1}(.)$ [24]. In (1j), the parameter a is defined to shorten (1i). In Set 1, parameters such as N and α separately relate to the precision and the width of the probability interval. Indeed, these are predefined parameters to achieve the desired results based on the operator's decision.

Finally, the CDFs of each X are calculated and its p-box can be constructed accordingly. With the proposed normalization function, the random values of Xs are transformed into the same range of numbers resulting in a proper analysis with the copula theory. The copula theory is a jointly modeling approach to achieve a single independent and identical distribution for Xs. This theory is utilized in order to tighten the probability interval and to increase the accuracy of the probability method, which leads to a better data-set. It should be mentioned that the utilization of copula theory does not contradict the imprecise nature of Xs and covers all possible occurrences [19]. The final output of the copula theory is the construction of an uncertainty set based on the posterior prognosticated distribution. According to this distribution, we generate a new data-set of a normalized number $\overset{*}{Norm}_X$. We apply copula density function to choose a posterior prognosticated distribution for each pair of Xs. In fact, N values of each paired X with the highest copula density are selected as $\overset{*}{Norm}_X$. With the inverse process of normalization function in (1b), (1c) realistic input samples for the proposed optimization framework can be achieved.

2) Aleatory Uncertainty Variables Modeling: For the second type of uncertainty variables (Ys), a probability-based method is proposed. We assume while modeling this type, the decision-maker has access to historical data for generating input samples. Subsequently, primary samples are generated based on these statistical data. Then, the LHS method is applied to estimate input values for the proposed optimization framework.

The LHS method is a satisfied-random procedure for sampling variables from a specific distribution [16]. Accordingly, there is a vector for each $Y \in \{Y_1, Y_2, ..., Y_{\tau 2}\}$ from a prescribed PDF. To select N samples, the LHS approach divides this vector into N subsets. Each subset is characterized by equal probability. The sampling process from each vector is dependent on the subset. LHS method is carried by transforming CDF of Y into the value with the inverse of the identical and independent normal PDF. The normal PDF of each Y is defined on the range of $[D_n, U_n]$ with $D_n = (n-1)/N$ and $U_n = n/N$. This procedure repeats N time for each Y.

B. Scenario Reduction

For total operation time horizon T, with assuming total number of uncertain variables is equal to summation of EUVs and AUVs numbers ($\tau = \tau_1 + \tau_2$) and generating N sample under proposed method, there is N^τ data-set at each t. Since this number is high, the complexity, running time and calculation burden of the problem are also increased. To alleviate this issue, we utilize SCENRED application which is applied with GAMS software to reduce the number of scenarios [25]. SCENRED is a useful solver of GAMS which can be applied when scenario reduction is needed in scenario-based stochastic optimization. The SCENRED solver utilizes a fast backward/forward technique to reach a small number of scenarios, which includes two algorithms, i.e. backward reduction and forward selection [26].

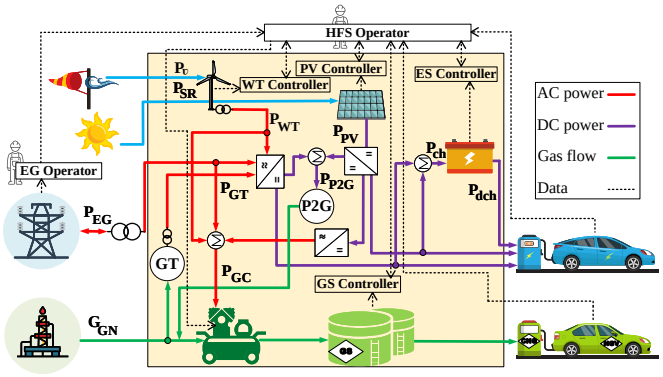

Fig. 2. Basic structure of the proposed HFS.

C. Configuration of the Proposed Station

In this section, the mathematical formulation of HFS assets is presented through (2)-(4). The overall structure of the HFS is depicted in Fig. 2. The HFS can be divided into three layers. The input layer includes received powers from an upstream electricity grid (P^t_{EG}), υ^t and SR^t as well as received gas volume from the urban gas network (G^t_{GN}). Then, in the interface layer, converters, power to gas system (P2G), gas turbine (GT) and compressor transform the input powers. In this layer, the HFS utilizes ES and gas storage (GS) to store multi-carrier energies. In the output layer, the HFS supplies EVs (L_{ev}) and NGVs load (L_{ngv}). Based on the type of energy, the constraints are divided into three main categories.

The first category includes the RESs, electricity grid, and ES as expressed in (2). The relationship between input (P^t_v) and output wind power (P^t_{WT}) of WT is presented in (2a). In which, we use the formulation applied in [1] to calculate the output power based on (υ^t). Also, power capacity limitation is depicted in constraint (2b). Similarly, the correlation between input SR power (P^t_{SR}) and output PV power (P^t_{PV}) as well as power capacity limitation of PV are modeled as (2c) and (2d). The exchanged power capacity between the proposed HFS and upstream electricity grid is demonstrated by (2e). The energy balance for ES charging (P^t_{ch}), discharging (P^t_{dch}), and exchangeable (P^t_{ex}) powers can be formulated as (2f). In (2g), by dispatchable power from PV, WT, upstream electricity grid, and GT modeled by dispatchable parameter γ the ES is charged through the AC/DC and DC/DC converters with predefined efficiency η_{Cs}. The maximum charge and discharge power limits are represented by (2h) and (2i). To avoid simultaneous charging and discharging, binary variable I^t_{ch}

SET 2 Electricity system model

$$P^t_{WT} = \eta_{WT}.P^t_v \qquad t \in [0,T] \tag{2a}$$
$$0 \le P^t_{WT} \le \overline{P}_{WT} \tag{2b}$$
$$P^t_{PV} = \eta_{PV}.P^t_{SR}.A \tag{2c}$$
$$0 \le P^t_{PV} \le \overline{P}_{PV} \tag{2d}$$
$$-\overline{P}_{EG} \le P^t_{EG} \le \overline{P}_{EG} \tag{2e}$$
$$P^t_{ex} = P^t_{ch}/\eta_{ES} + \eta_{ES}.P^t_{dch} \tag{2f}$$
$$P^t_{ch} = \gamma.\eta_{Cs}.[(P^t_{PV} + P^t_{WT} + P^t_{EG}) + P^t_{GT}] \tag{2g}$$
$$0 \le P^t_{ch} \le I^t_{ch}.\overline{P}_{ch} \qquad I^t_{ch} \in \{0,1\} \tag{2h}$$
$$0 \le P^t_{dch} \le (1 - I^t_{ch}).\overline{P}_{dch} \tag{2i}$$
$$SoC^{t+1} = SoC^t + [P^t_{ch}.\eta_{ES} - P^t_{dch}/\eta_{ES}] \tag{2j}$$
$$\underline{SoC} \le SoC^t \le \overline{SoC} \tag{2k}$$
$$SoC^{t=0} = SoC^{t=T} \tag{2l}$$

SET 3 Coordination constraints

$$G^t_{P2G} = \eta_{P2G}.P^t_{P2G} \tag{3a}$$
$$P^t_{P2G} = \delta.\eta_{Cs}.[P^t_{WT} + P^t_{PV} + P^t_{EG}] \qquad \forall\delta \in [0,1] \tag{3b}$$
$$0 \le P^t_{P2G} \le \overline{P}_{P2G} \tag{3c}$$
$$P^t_{GT} = \eta_{GT}.\lambda.G^t_{GN} \quad \forall\lambda \in [0,1] \tag{3d}$$
$$0 \le P^t_{GT} \le \overline{P}_{GT} \tag{3e}$$
$$G^t_{out,GC} = \eta_{GC}.P^t_{GC} \tag{3f}$$
$$P^t_{GC} = \varrho.[P^t_{WT} + \eta_{Cs}.P^t_{PV} + P^t_{EG}] \qquad \forall\varrho \in [0,1] \tag{3g}$$
$$0 \le P^t_{GC} \le u^t.\overline{P}_{GC} \qquad u^t \in \{0,1\} \tag{3h}$$
$$G^t_{out,GC} = CF.G^t_{in,GC} \tag{3i}$$
$$G^t_{in,GC} = (1-\lambda).G^t_{GN} \tag{3j}$$

is introduced in constraint (2h). I^t_{ch} is equal to one when charging mode is on. Additionally, the relationship between charging or discharging power and state of charge (SOC^t) is presented in (2j). The state of charge is limited by (2k). To ensure that the state of charge at the beginning and end of optimization period is equal, the constraint in (2l) is considered.

The operation constraints of the P2G, GT, and compressor which coordinate electricity and natural gas are formulated as the same category in (3). The P2G converting process of electricity power (P^t_{P2G}) to natural gas flow (G^t_{P2G}), are modeled as shown in (3a). In (3b), the P2G input power is supplied utilizing dispatchable power of WT, PV, and electricity grid constrained with (3c). The GT output power (P^t_{GT}) is generated by converting dispatchable natural gas from urban gas network (G^t_{GN}) in (3d) and limited by (3e). As stated in (3f), the output CNG from the compressor ($G^t_{out,GC}$) mainly depends on received dispatchable power (P^t_{GC}) from WT, PV, electricity grid, and ES modeled by dispatchable parameter ϱ in (3g) and limited in (3h). To extend the expected lifetime and reducing maintenance cost of compressor, we define auxiliary binary variable u^t in which is 1 if compressor

SET 4 Gaseous system model

$$0 \le G^t_{GN} \le \overline{G}_{GN} \tag{4a}$$
$$W^t_s = W^{t=0}_s + \sum\nolimits_{t=1}^{T} \left(W^t_{in} - W^t_{out}\right) \tag{4b}$$
$$\underline{W}_s \le W^t_s \le \overline{W}_s \tag{4c}$$
$$W^{t=0}_s = W^{t=T}_s \tag{4d}$$

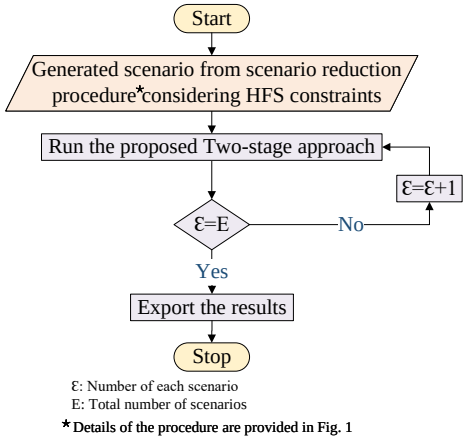

Fig. 3. Summary of the optimization process.

is switched on. In (3i) the pressure of output CNG from the compressor depends on CF as a compression factor. In (3j), the compressor input gas ($G^t_{in,GC}$) is supplied by dispatchable gas flow from urban gas network.

The gaseous constraints include urban gas network and GS specified as (4). Where W_s is stored gas weight in the GS. Accordingly, the supplied natural gas from the urban gas network is limited by (4a). The stored CNG in the GS is related to input gas weight (W^t_{in}) and output gas weight (W^t_{out}) quantified by (4b) and limited in (4c). The constraint in (4d) guarantees the equality of the stored gas at the beginning and ending of the optimization period. Since there is a unilateral path for connecting the compressor, GS and NGVs, GS's input and output gas are limited. Besides, the type of gas is CNG, the capacity of GS is relatively low, and GC compresses the gas whenever sense the pressure drop, even NGVs are refueling. Hence, the gas in the proposed GS can be practically stored and used simultaneously.

The introduced HFS is implemented by energy transformation, redistribution, and storage among different types of energies. Hence, the mathematical model of the HFS as well as converting the relationship between the input and output energies can be expressed as (5). Accordingly, the coupling matrix H is considered as constant coefficient constructed based on components efficiencies and dispatchable factors to connect received energies in the input layer (P^t_{in}) and supplied demand power in the output layer (P^t_{out}) as (5a). Regarding connections in Fig. 2, the relationship in (5a) is rewritten as (5b)-(5d). Where, the dispatch factors γ, λ, δ and ϱ are predefined parameters determined by HFS operator.

SET 5 HFS model

$$[P_{out}] = [H] \times [P_{in}] \tag{5a}$$

$$\begin{bmatrix} L_{ev}^t \\ L_{ngv}^t \end{bmatrix} = \begin{bmatrix} H_e & H_{ge} \\ H_{eg} & H_g \end{bmatrix} \times \begin{bmatrix} P_e^t \\ G_{GN}^t \end{bmatrix} \tag{5b}$$

$$\begin{cases} H_e = \eta_{Cs}\left(1+\eta_{PV}+\eta_{WT}\right)+\left(\gamma\eta_{ES}+1-\gamma\right) \\ H_{ge} = \lambda\eta_{GT}\eta_{Cs}\left(\gamma\eta_{ES}+1-\gamma\right) \\ H_{eg} = \left(\delta\eta_{P2G}+\varrho\eta_{GC}\right)\left(1+\eta_{WT}+\eta_{PV}\eta_{Cs}^2\right) \\ H_g = \left(1-\lambda\right)\eta_{GC} \end{cases} \tag{5c}$$

$$P_e^t = P_{WT}^t + P_{PV}^t + P_{EG}^t \tag{5d}$$

SET 6 Two-stage optimal operation

$$Min \sum_{t=1}^{T}\left[E_1\left(\omega_1^t\right)+\sum_{\varepsilon=1}^{E}\pi_\varepsilon.E_{1|2}\left(\omega_{1|2}^t\right)\right] \tag{6a}$$

$$+\beta.\xi_{CVaR}$$

s.t.:

$$E_1\left(\omega_1^t\right) = CC^t + SC^t \tag{6b}$$

$$CC^t = y^t.SU + z^t.SD \tag{6c}$$

$$y^t - z^t = u^t - u^{t-1} \tag{6d}$$

$$y^t + z^t \le 1 \tag{6e}$$

$$SC^t = I_{ch}^t SCC + I_{dch}^t SDC \tag{6f}$$

$$E_{1|2}\left(\omega_{1|2}^t\right) = PC_\varepsilon^t + GC_\varepsilon^t + LC_\varepsilon^t \tag{6g}$$

$$PC_\varepsilon^t = C_e^t.P_{EG,\varepsilon}^t \tag{6h}$$

$$GC_\varepsilon^t = C_g^t.G_{GN,\varepsilon}^t \tag{6i}$$

$$LC_\varepsilon^t = \rho\left(C_e^t.L_{ev,\varepsilon}^t\right) \tag{6j}$$

$$\xi_{CVaR} = \xi_\alpha + \frac{1}{1-\alpha}\sum_{\varepsilon=1}^{E}\pi_\varepsilon.p_\varepsilon \tag{6k}$$

$$\sum_{t=1}^{T}\left[\sum_{\varepsilon=1}^{E}\pi_\varepsilon.E_{1|2}\left(\omega_{1|2}^t\right)\right] - \xi_\alpha \le p_\varepsilon \tag{6l}$$

$$(2)-(5) \tag{6m}$$

III. The Proposed Optimization Framework

The objective function of the optimal operation framework of the HFS is expected day ahead (DA) operation costs demonstrated in (6). We employ a two-stage decision-making approach to solve this problem as shown in Fig. 3. Indeed, the operation of all components is classified into two different types: deterministic (scenario-independent) and stochastic (scenario-dependent), resulting in a two-stage approach. The first type of components is considered as the first-stage to minimize the ES's charging and discharging number stated by binary variables, i.e., I_{ch}^t, I_{dch}^t as well as the unit-commitment binary variables to constraint the compressor's turning-on and turning-off situation, i.e., y^t, u^t, z^t under a deterministic framework. As well, the second type components including scenario-based day-ahead decision-making variables to achieve minimum stochastic operation cost, i.e., P_{EG}^t, G_{GN}^t, L_{ev}^t and risk analyzing ξ_{CVaR} are considered as second stage problems. The deterministic variables from the first-stage are considered as input parameters for each scenario of the second-stage to implement the interconnection between the proposed solution methodology stages.

In (6a), different stages of the proposed approach are presented by $E_1(.)$ and $E_{1|2}(.)$ in which the optimal decision in the second stage depends on the results of the first stage. In addition, $\varepsilon = \{1, 2, 3, ..., E\}$ is number of each scenario, π_ε is stochastic probability of each scenario in which $\sum_{\varepsilon=1}^{E}\pi_\varepsilon = 1$, β is risk factor, and ξ_{CVaR} is CVaR with confident level α. The decision variables of each stage ω_1 and $\omega_{1|2}$ are shown in (6b) and (6g).

The first-stage decision variables are scenario-independent variables to represent the basic two damageable components under various status changes. Hence, the decision variables in the first stage are included in the compressor operation cost CC^t and electricity storage operation cost SC^t. To minimize the compressor switching number between on or off state, we model compressor operation by defining two binary variables y^t and z^t in (6c)-(6e). Where, SU and SD are compressor start-up and shut-down costs, respectively. In (6f) the ES charging SCC^t or discharging cost SDC^t is modeled. These variables are determined before incorporating random samples and generating realization scenarios. Thus, they are constant in all scenarios.

The second-stage is run with incorporating uncertainty variables to make a decision about purchased power from upstream distribution system PC^t and purchased natural gas from urban gas network GC^t are indicated in (6h) and (6i), respectively. Where, C_e^t and C_g^t are prices of electricity and natural gas. In (6j), the cost of participated load demand LC^t in a price-based DRP is modelled where ρ is participation rate of EVs in the DRP. The decision variables of the second stage are scenario-based to determine the real-time scheduling RESs and other components operation.

Considering the uncertainty of the HFS operator decision-making problem needs a risk measurement wherein our work is provided with the conditional value-at-risk (CVaR) to manage financial risks and uncertainties as demonstrated in (6k) and (6l); where, ξ_α is an auxiliary variable for calculating CVaR criterion ξ_{CVaR} with confidence level α. The auxiliary variable $p_\varepsilon \in \mathbb{R}_+$ determines the range of differences between the expected DA operation cost and ξ_α in each scenario.

To summarize, the overall objective function of HFS optimal operation in (6a) aims to reduce costs considering risk analyses through the different values for the β parameter. Scenario-independent costs related to the operation statuses of ES and compressor are presented in (6b)-(6f). Besides, scenario-based costs are calculated based on defining CVaR in (6g)-(6l). The inclusion of the weighted correction factor β varied from 0 to 1, indicates the balance between risk and expected costs. Therefore, to calculate these scenario-dependent and scenario-independent costs, the variables are optimized as a two-stage approach according to Fig. 4

IV. Case Study

In order to investigate the proposed two-stage optimization for the daily operation of the HFS numerical studies are carried

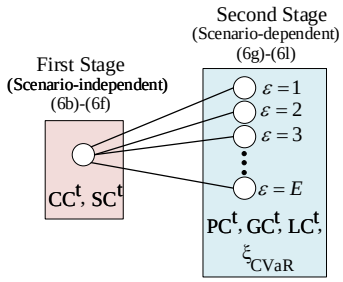

Fig. 4. Scenario-tree for the proposed two-stage approach.

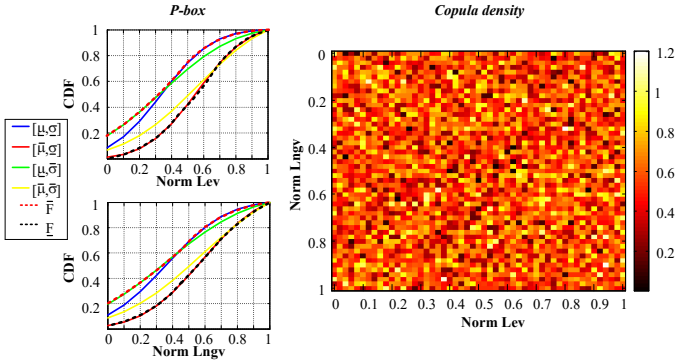

Fig. 5. EUVs modeling: p-box construction and copula density function calculation to generate new normalized values for EUVs at t=40.

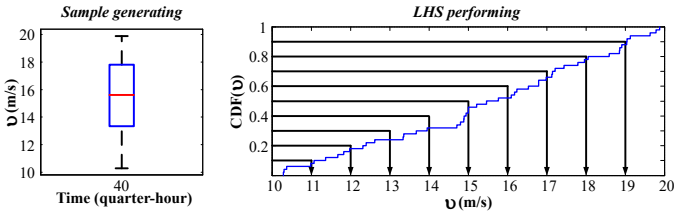

Fig. 6. AUVs modeling: samples are generated for wind speed under predefined limitations then LHS method is applied based on the CDFs at t=40. The same approach is employed for other AUVs for each time slot.

out over the course of a day as demonstrated in the following subsections.

A. Input Data

Targeting higher accuracy, the operation time is split into time intervals of 15-minute (T=96). Also, there are 10 chargers and CNG dispensers in the HFS. The data of C_e^t and C_{GN}^t are obtained from [27] and [6]. The maximum rated power capacity of WT, PV, P2G, compressor, GT, ES and converters are 80 kW, 50 kW, 100 kW, 400 kW, 100 kW, 20 kW and 500 kW, respectively. The maximum exchanged power with the electricity grid is 500 kW and the maximum received natural gas volume from the urban gas network is 1 Mm^3/month. Other data such as WT parameters and efficiency of components are in accordance with [10], [20], [28].

We assume that before construction of the HFS, there is no exact information about drivers refueling behavior as well as the number of EVs and NGVs. The random values of initial and final SOCs cause uncertainty in parameter L_{ev}. Similarly, initial and final CNG values of NGVs lead to uncertain L_{ngv}. We consider 10 charging sockets with fast charging rate of 60 kW DC and maximum charging time 20 min [29]. Also, there are 10 CNG dispensers to fully refuel an empty NGV with CNG capacity of 7 kg in a 5 min period. Accordingly, in the proposed optimization framework, the uncertain L_{ev} and L_{ngv} are modeled as EUVs (τ_1=2) where the only information available for these parameters is the power for supplying capacity of the HFS. Therefore, the extreme vertexes of the set which these parameters can realize within is identified as $\left[\underline{L}_{ev}, \overline{L}_{ev}\right]$ and $\left[\underline{L}_{ngv}, \overline{L}_{ngv}\right]$ and set to $[0, 450]$ kW and $[0, 35]$ kg to generate 100 random samples by Monte Carlo method. Considering different natures, limitations, and units of these EUVs, the proposed two-step normalization function in (1b) and (1c) is utilized in HFS scheduling. Generated random samples are transformed into a range of $[0, 1]$. Afterward, the values of μ and σ are determined as explained in equations (1d) and (1e) for each time slot. To construct the p-boxs the limitations of $\left[\underline{\mu}, \overline{\mu}\right]$ and $\left[\underline{\sigma}, \overline{\sigma}\right]$ are calculated by applying (1g)-(1j). For instance, the imprecise characterization of primary samples are illustrated by p-box in Fig. 5 for confidence level 95%. The random area between bounds can be employed as a non-parametric model of variability for each EUV. To tighten the space between $\left[\underline{F}, \overline{F}\right]$ and to generalize a single data-set for the proposed EUVs, the copula theory is employed. The EUVs include the variables of EHs output layer for supplying L_{ev}^t and L_{ngv}^t. The output energy carriers are related to each other by utilizing P2G and NGDG. Thus, based on this interdependency, the copula theory is applied to handle Xs. Furthermore, since the generated data for EUVs are transformed into the similar range of [0,1] by normalized functions in (1b) and (1c), the copula theory can be directly utilized without considering the correlation matrix between Xs. In this regard, we use Gaussian copula to connect p-boxes of both EUVs [19]. As a result, 10 pair that coordinate with the maximum copula density are chosen as $\overset{*}{Norm}_{L_{ev}}$ and $\overset{*}{Norm}_{L_{ngv}}$. For instance, as shown in Fig. 5, these target samples are the pair coordinates with the whitest color. Eventually, the final 10 stochastic samples for each EUV are yielded by applying inverse normalization function.

For the probability-based modeling of AUVs, we utilize LHS technique to obtain samples of v^t and SR^t. At each t, the generated samples for v and SR follow Gaussian and beta distribution functions, respectively. Furthermore, in order to visually indicate the range of variations for distribution functions, a box-plot of the samples is represented in Fig. 6 based on historical data. This figure is an example of 50 generated samples at t=40 to obtain 10 samples which cover all portions of the distribution; the CDF of each AUV is divided into N=10 sub-set with an equal probability of 0.1. Then, a unique sample is chosen from each determined sub-sets.

By gathering selected samples in each t, the scenarios are generated for all of the operation time horizons. Given that N=10, τ_1=2 and τ_2=3, the total number of scenarios is 10^5.

Note that, when necessary, to have better comprehensibility, the unit of purchased gas is converted from m^3 into kWh

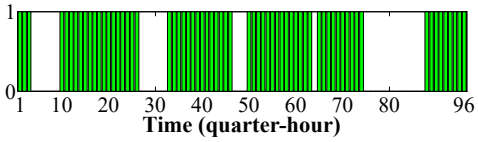

(a) u

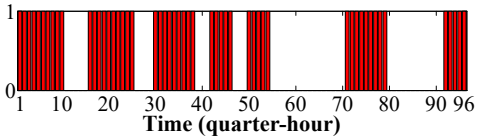

(b) $I_{ch/dch}$

Fig. 7. Optimal operational intervals for GC and ES.

utilizing the low heating value of natural gas. The MATLAB software is used for the sample gathering and SCENRED is utilized to reduce the number of scenarios to 100. The proposed optimization framework is an MILP problem solved by the CPLEX solver of GAMS software on a PC with Intel core i5, 320 GHz and 4GB of RAM.

B. Results of the first stage

As mentioned previously optimization has two stages where the outputs of the first stage are binary variables: I^t_{ch}, I^t_{dch}, u^t, y^t, z^t. Indeed, these variables determine a fixed scheduling for both ES and GC. For instance, Fig. 7a shows a constant either switching on or switching off statements of compressor to avoid damaging it. In addition, the fix utilization program is determined for ES either charging or discharging statements to increase ES life spam and decrease its amortization schedule as presented in Fig. 7b. The results of first stage are scenario independent.

C. Results of the Second Stage

The values of the first stage decision variables are utilized as inputs for the stochastic operation framework in the second stage. In Fig. 8, the interactions of the proposed HFS with the upstream electricity grid and urban gas network are illustrated as second stage decision variables. It can be concluded that at the beginning and ending of DA, the optimal operation horizon purchased power is almost zero. This is due to the high generation available from wind generation. It can be perceived that the purchased power is significantly decreased at $t = [53, 73]$ in which the demand is supplied by generated power from PV. Furthermore, in the high price time range, $t = [73, 88]$ the received gas is maximized to utilize GT in order to sell more electric power to the electric market.

Fig. 9, Fig. 10 and Fig. 11 show the stored gas variation in the GS, coordination procedure, and ES optimal operation, respectively. Note that, in Fig. 9 growth or decrement of the gas weight in GS is dependent on the compressor operation and NGVs demand. For instance, the optimal commitment of the compressor is determined from the first stage. Hence, the HFS operator turns off compressor at high energy price $t = [70, 89]$. In Fig. 10, the forecasted participation scheduling of the jointing units GT and P2G depends on the real time pricing (RTP) and generated power from RESs. In Fig. 11, the

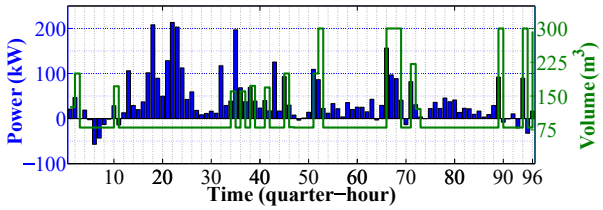

Fig. 8. Exchanged power with the electricity grid and purchased gas volume from urban gas network.

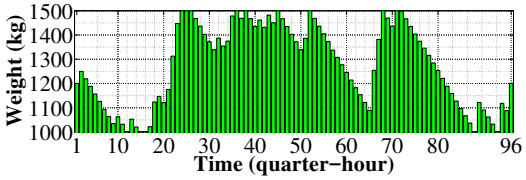

(a) W_s

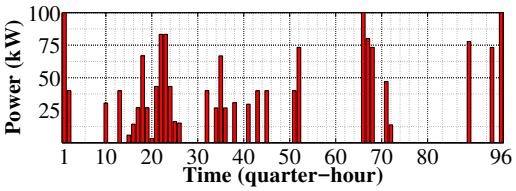

(b) P_{GC}

Fig. 9. Optimal scheduling of GC and GS for desired CNG supplying.

operation principles of ES are presented according to obtained results from the first stage. Due to the higher power price, the ES charging rate in the range of $t = [53, 93]$ is equal to zero. Controversy, the value of ES discharging power in the high price moments is increased effectively.

Fig. 12 shows the variation of two financial variables of CVaR versus expected DA operation cost of HFS provided for different values of β. The trade-off between the optimal operation cost and cost variability from CVaR point of view is modeled by modifying β parameter in the range of [0,1]. The

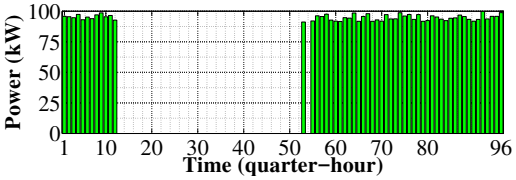

(a) P_{GT}

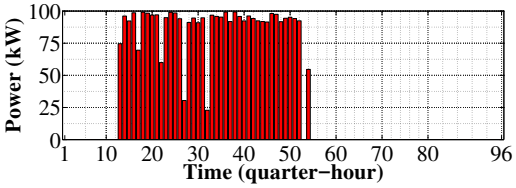

(b) P_{P2G}

Fig. 10. Optimal operation of jointing units.

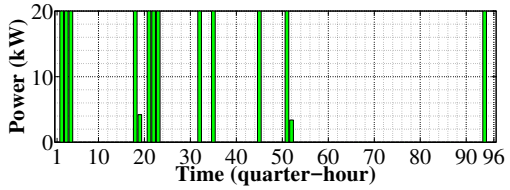

(a) P_{ch}

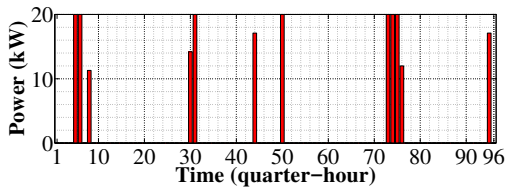

(b) P_{dch}

Fig. 11. Optimal operation of ES.

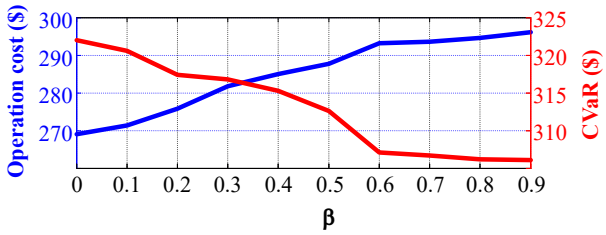

Fig. 12. Expected operation cost of the HFS versus CVaR cost under various risk weighting factor β.

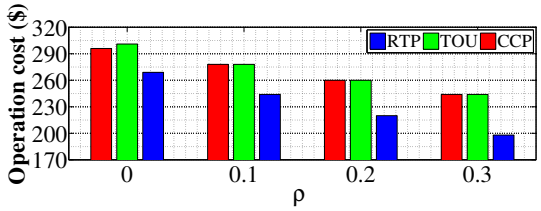

Fig. 13. Comparing of the HFS expected operation cost with applying different price-based DRPs for various EVs participation rates.

highest CVaR value is obtained in β=0. The highest optimal operation cost is obtained in β=1. Given that β increases from 0 to 1, the HFS operation cost increases from 269 $ to 296 $ (10%), while CVaR decreases from 322 $ to 306 $ (5%). These results illustrate an adequate trade-off between operation and risk costs. Indeed, with increasing the operation cost, the risk cost can be efficiently reduced. In addition, a higher risk factor $0.6 \leq \beta \leq 1$ does not extremely affect neither operation nor risk costs. Hence, the proper range to control trade-off between these financial variables is $0 < \beta < 0.6$.

Finally, in order to study the DA operational specifics of the HFS, different price-based DRPs and participation rates are compared in Fig. 13. In this regard, two other types of DA energy pricing method time of use (TOU) and critical peak pricing (CPP) are taken into account in which their tariffs are in accordance with [12]. Considering the mean of RTP in the peak tariff hours [16,24) which equals to 0.11 $/kWh, we define three ranges for TOU as valley tariff 0.027 $/kWh

TABLE II
THE COMPARISON OF OPERATION COSTS BASED ON DIFFERENT UNCERTAINTY MODELING METHODS (β, ρ=0).

Day	Optimal operation cost ($)					
	Proposed	Stochastic adaptive robust [31]			Pure stochastic [20]	Deterministic
		Γ=0.2	Γ=0.4	Γ=0.6		
1	265.253	271.144	270.687	268.214	274.614	281.076
2	261.332	268.465	264.655	261.741	272.216	277.576
3	269.213	271.901	270.214	266.576	279.910	288.047
4	275.702	279.259	279.860	277.102	283.357	292.164

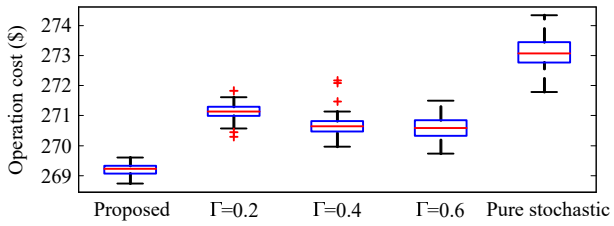

Fig. 14. Comparison of different methods in terms of optimal operation cost for alternative decisions by HFS operator (β, ρ=0)

within [0,8), off-peak tariff 0.055 $/kWh within [8,16) and peak tariff 0.11 $/kWh within [16,24). The tariffs in CCP is similar to TOU, except for a critical peak within [18,22] is equal to the maximum RTP 0.28 $/kWh. To compare various price-based DRPs, operation costs of HFS are presented under different EVs participating rate in each DRP. As can be seen, by increasing the participation rate, the operation costs of HFS in both TOU and CPP are almost similar. This is due to the fact that the HFS operator is able to utilize various options to supply EVs as well as peak shifting. It is clear that the proper DRP for our HFS is RTP-based DRP.

D. Comparative Analysis

In order to verify the economic benefits of our HFS structure, we compare it with a conventional HFS. In the conventional fuel stations, we assume that RESs, P2G, GT are absent, and each type of demand is supplied independently. By running the optimization process, the operation cost of the proposed HFS for the worst scenario is 277 $ in a whole day. However, the operation cost for the mentioned conventional HFS is 921 $ over the course of a day. Even if we add all capital costs of PV, WT, GT, ES and P2G from available studies such as [30], the payback period would be around 26 months. This proves the economic precedence of the introduced structure.

Additionally, in order to verify the effectiveness and efficiency of the proposed uncertainty modeling approach, we compare it with the most similar ones in the literature, namely stochastic adaptive robust [31], pure stochastic [20], and deterministic method. In so doing, we run the problem of HFS scheduling with each optimization method considering 100 scenarios generated by Monte Carlo simulation. Note that, for the deterministic approach, expected values of each uncertain parameter are utilized. For the stochastic adaptive robust method, the uncertainty budget can noticeably affect the outcomes. Therefore, three uncertainty budgets (Γ=0.2,0.4,0.6) are considered for the sake of a better comparison. The expected HFS scheduling costs of four different days are

TABLE III
RESULTS OF THE PROPOSED METHOD FOR VARIOUS NUMBER OF SCENARIOS

E	5	10	50	100	150	200
Operation Cost ($)	279.3	268.7	264.9	262.7	261.7	261.1
CPU time (s)	1.73	2.62	19.7	47.6	91.8	358

TABLE IV
SPECIFICATIONS OF DIFFERENT PROBABILITY DENSITY FUNCTIONS

PDF	Skewness	Kurtosis	Std	Median
Beta (BE)	-1.921	6.832	0.111	0.9325
Gamma (GM)	1.394	5.452	0.103	0.119
Gaussian (GU)	1.244	4.4503	0.0869	0.513
Normal (NO)	-0.058	2.795	0.096	0.492
Weibull (WE)	-0.354	2.510	0.885	0.479

given in Table II for the aforementioned approaches. As can be seen, the deterministic approach has the worst results, and stochastic adaptive robust optimization is doing better than full stochastic. However, for different uncertainty budgets, different results are observed. Table II demonstrates the effectiveness of the proposed method as it achieves better results compared to the other approaches. Note that, when the budget of uncertainty is considered to be 0.6 in day 3, the cost of stochastic adaptive robust optimization is less than the proposed approach. However, the acquired results are expected values. So, to further investigate the results, we have provided an out of sample analysis for which we assume that first stage results are fixed, and we generate new 100 scenarios for the uncertain parameters. Then, we run only the second stage to acquire the scheduling cost of HFS for a typical day. The boxplots related to each method are depicted in Fig. 14. It is clear that for out of sample data, the proposed approach achieves the lowest costs. Thus, in conclusion, our proposed approach can outperform the existing uncertainty modeling methods in case of an HFS, which deals with multiple sources of uncertainty.

It is worthy of mentioning that in both economic and uncertainty modeling comparisons, the optimization process is applied without participating in DRP and risk analyses. Also, to have a reasonable comparison, the number of generated scenarios for each method is equal to 100.

To further verify the effectiveness of the proposed MILP two-stage approach, the expected operation cost and the calculation time with respect to the number of scenarios generated by SCENRED are presented in Table III. The operation cost of HFS converges at almost 263 $ for different values of E. It is clear that for more than 100 scenarios, there is a negligible difference among results. Accordingly, an increase in the number of scenarios will lead to unnecessary and excessive computation burdens. In order to achieve an appropriate balance between the objective function values and calculation times, 100 scenarios have been selected for analyses.

For testing the effect of PDFs on HFS's operation cost evaluation various comparisons have been obtained considering the specifications in Table IV. To achieve a fair comparison among PDFs the standard division (Std) of them are considered 10% with a tolerance of $\pm 2\%$. The evaluated operation cost based on estimated data for AUVs , i.e. υ and SR, by different

TABLE V
COMPUTATIONAL ERRORS OF EXPECTED OPTIMAL OPERATION COST FOR DIFFERENT PROBABILITY DENSITY FUNCTIONS

Variable		Error			Variable		Error		
υ	SR	KS test	RMSE	χ^2	υ	SR	KS test	RMSE	χ^2
BE	GM	0.0164	0.0061	0.0182	GM	NO	0.0311	0.0123	0.0454
GM	BE	0.0132	0.0058	0.0138	NO	GM	0.0457	0.0289	0.0690
BE	GU	0.0211	0.0076	0.0247	GM	WE	0.0941	0.0534	0.2130
GU	BE	0	0	0	WE	GM	0.0707	0.0458	0.1533
BE	NO	0.1031	0.0689	0.2190	GU	NO	0.0520	0.0319	0.0661
NO	BE	0.0367	0.0152	0.0456	NO	GU	0.0629	0.0361	0.0864
BE	WE	0.0420	0.0281	0.0606	GU	WE	0.0161	0.0051	0.0168
WE	BE	0.0140	0.0055	0.0171	WE	GU	0.017	0.0046	0.0147
GM	GU	0.0907	0.0511	0.1973	NO	WE	0.0312	0.0128	0.0432
GU	GM	0.0632	0.0376	0.0764	WE	NO	0.0412	0.0156	0.0512

PDFs are compared considering three kinds of statistical errors Kolmogorov-Smirnov (KS) test, root mean square error (RMSE), and Chi-square error (χ^2) [32] . As a result, Table V lists the values computed for different PDF combinations of AUVs. These errors are calculated by assuming the expected cost 265.253 $ obtained from GU and BE PDFs as actual value (Table II); so, the errors for these PDFs are zero. As shown in Table V, the maximum errors of KS test, RMSE, and χ^2 is calculated as 10%, 6.8%, and 21%, respectively. The calculated values for all error indices indicate that all PDFs are matched well with the assumed actual value. Consequently, the value of the expected operation cost is quite consistent with the calculated one due to the flexibility of HFS against uncertainties by utilizing multiple power sources.

V. Conclusion

There are many real-world applications that deal with several uncertainty sources while trying to reach an optimized performance. These uncertainties generally stem from two reasons: lack of previously known data and randomness in behavior. In this study, we introduced a mathematical framework to separate types of uncertainties and employ proper modeling while dealing with each type. To apply the proposed optimization framework in a real-world application, we considered an HFS that utilizes the energy hub structure and several converters to supply EVs along with NGVs. The HFS received electric power from the network, urban natural gas grid and renewable energy sources, and converted them through electric converters, the power to gas system and gas turbine to supply demands. The HFS deals with multiple uncertainties with different natures. In this regard, a two-stage stochastic optimization was carried based on the proposed uncertainty modeling. The applicability and effectiveness of the introduced method were shown through numerical studies. It was concluded with an out-of-sample analysis that the proposed method could even outperform famous existing approaches in the literature, including stochastic adaptive robust approach.

References

[1] B. Faridpak, A. Alahyari, M. Farrokhifar, and H. Momeni, "Toward small scale renewable energy hub-based hybrid fuel stations: Appraising structure and scheduling," *IEEE Transactions on Transportation Electrification*, vol. 6, no. 1, pp. 267–277, 2020.

[2] M. Farrokhifar, Y. Nie, and D. Pozo, "Energy systems planning: A survey on models for integrated power and natural gas networks coordination," *Applied Energy*, vol. 262, p. 114567, 2020.
[3] M. Moeini-Aghtaie, A. Abbaspour, M. Fotuhi-Firuzabad, and P. Dehghanian, "Optimized probabilistic PHEVs demand management in the context of energy hubs," *IEEE Transactions on Power Delivery*, vol. 30, no. 2, pp. 996–1006, 2014.
[4] C. Shao, X. Wang, M. Shahidehpour, X. Wang, and B. Wang, "An MILP-based optimal power flow in multicarrier energy systems," *IEEE Transactions on Sustainable Energy*, vol. 8, no. 1, pp. 239–248, 2017.
[5] M. Rastegar, M. Fotuhi-Firuzabad, H. Zareipour, and M. Moeini-Aghtaieh, "A probabilistic energy management scheme for renewable-based residential energy hubs," *IEEE Transactions on Smart Grid*, vol. 8, no. 5, pp. 2217–2227, 2017.
[6] W. Zhong, C. Yang, K. Xie, S. Xie, and Y. Zhang, "ADMM-based distributed auction mechanism for energy hub scheduling in smart buildings," *IEEE Access*, vol. 6, pp. 45 635–45 645, 2018.
[7] M. Moeini-Aghtaie, A. Abbaspour, M. Fotuhi-Firuzabad, and E. Hajipour, "A decomposed solution to multiple-energy carriers optimal power flow," *IEEE Transactions on Power Systems*, vol. 29, no. 2, pp. 707–716, 2013.
[8] H. R. Massrur, T. Niknam, and M. Fotuhi-Firuzabad, "Investigation of carrier demand response uncertainty on energy flow of renewable-based integrated electricity–gas–heat systems," *IEEE Transactions on Industrial Informatics*, vol. 14, no. 11, pp. 5133–5142, 2018.
[9] S. Moazeni, A. H. Miragha, and B. Defourny, "A risk-averse stochastic dynamic programming approach to energy hub optimal dispatch," *IEEE Transactions on Power Systems*, vol. 34, no. 3, pp. 2169–2178, 2018.
[10] D. Huo, C. Gu, K. Ma, W. Wei, Y. Xiang, and S. Le Blond, "Chance-constrained optimization for multienergy hub systems in a smart city," *IEEE Transactions on Industrial Electronics*, vol. 66, no. 2, pp. 1402–1412, 2018.
[11] M. Yazdani-Damavandi, M. P. Moghaddam, M.-R. Haghifam, M. Shafie-khah, and J. P. Catalão, "Modeling operational behavior of plug-in electric vehicles parking lot in multienergy systems," *IEEE Transactions on Smart Grid*, vol. 7, no. 1, pp. 124–135, 2015.
[12] M. Shafie-khah, E. Heydarian-Forushani, G. J. Osório, F. A. Gil, J. Aghaei, M. Barani, and J. P. Catalão, "Optimal behavior of electric vehicle parking lots as demand response aggregation agents," *IEEE Transactions on Smart Grid*, vol. 7, no. 6, pp. 2654–2665, 2015.
[13] H.-M. Chung, W.-T. Li, C. Yuen, C.-K. Wen, and N. Crespi, "Electric vehicle charge scheduling mechanism to maximize cost efficiency and user convenience," *IEEE Transactions on Smart Grid*, vol. 10, no. 3, pp. 3020–3030, 2018.
[14] Q. Yan, B. Zhang, and M. Kezunovic, "Optimized operational cost reduction for an EV charging station integrated with battery energy storage and PV generation," *IEEE Transactions on Smart Grid*, vol. 10, no. 2, pp. 2096–2106, 2018.
[15] C. Kagiri, E. M. Wanjiru, L. Zhang, and X. Xia, "Optimized response to electricity time-of-use tariff of a compressed natural gas fuelling station," *Applied Energy*, vol. 222, pp. 244–256, 2018.
[16] N. F. Avila and C.-C. Chu, "Distributed probabilistic ATC assessment by optimality conditions decomposition and LHS considering intermittent wind power generation," *IEEE Transactions on Sustainable Energy*, vol. 10, no. 1, pp. 375–385, 2018.
[17] Y. Li, T. Zhao, C. Liu, Y. Zhao, Z. Yu, K. Li, and L. Wu, "Day-ahead coordinated scheduling of hydro and wind power generation system considering uncertainties," *IEEE Transactions on Industry Applications*, vol. 55, no. 3, pp. 2368–2377, 2019.
[18] Y. Li, P. Wang, H. B. Gooi, J. Ye, and L. Wu, "Multi-objective optimal dispatch of microgrid under uncertainties via interval optimization," *IEEE Transactions on Smart Grid*, vol. 10, no. 2, pp. 2046–2058, 2017.
[19] M. Cui, V. Krishnan, B. Hodge, and J. Zhang, "A copula-based conditional probabilistic forecast model for wind power ramps," *IEEE Transactions on Smart Grid*, vol. 10, no. 4, pp. 3870–3882, 2019.
[20] B. Zhou, D. Xu, C. Li, C. Y. Chung, Y. Cao, K. W. Chan, and Q. Wu, "Optimal scheduling of biogas-solar-wind renewable portfolio for multicarrier energy supplies," *IEEE Transactions on Power Systems*, vol. 33, no. 6, pp. 6229–6239, 2018.
[21] Y. Hou, M. Sallak, and W. Schön, "Estimation of imprecise reliability of systems using random sets and monte carlo resampling procedures," *IEEE Transactions on Systems, Man, and Cybernetics: Systems*, vol. 47, no. 11, pp. 2844–2855, 2016.
[22] M. H. Barmayoon, M. Fotuhi-Firuzabad, A. Rajabi-Ghahnavieh, and M. Moeini-Aghtaie, "Energy storage in renewable-based residential energy hubs," *IET Generation, Transmission & Distribution*, vol. 10, no. 13, pp. 3127–3134, 2016.
[23] A. Alahyari, M. Ehsan, D. Pozo, and M. Farrokhifar, "Hybrid uncertainty-based offering strategy for virtual power plants," *IET Renewable Power Generation*, vol. 14, no. 13, pp. 2359–2366, 2020.
[24] J. L. Devore, *Probability and Statistics for Engineering and the Sciences*. Cengage learning, 2011.
[25] "GAMS development corp." https://www.gams.com.
[26] J. Li, F. Lan, and H. Wei, "A scenario optimal reduction method for wind power time series," *IEEE Transactions on Power Systems*, vol. 31, no. 2, pp. 1657–1658, 2015.
[27] J. Yang, J. Zhao, F. Wen, and Z. Dong, "A model of customizing electricity retail prices based on load profile clustering analysis," *IEEE Transactions on Smart Grid*, vol. 10, no. 3, pp. 3374–3386, 2018.
[28] K. Chaudhari, A. Ukil, K. N. Kumar, U. Manandhar, and S. K. Kollimalla, "Hybrid optimization for economic deployment of ESS in PV-integrated EV charging stations," *IEEE Transactions on Industrial Informatics*, vol. 14, no. 1, pp. 106–116, 2018.
[29] T. G. Alghamdi, D. Said, and H. T. Mouftah, "Decentralized electric vehicle supply stations (D-EVSSs): A realistic scenario for smart cities," *IEEE Access*, vol. 7, pp. 63 016–63 026, 2019.
[30] "Energy information administration of U.S." https://www.eia.gov, accessed: 2019-01-30.
[31] A. Baringo and L. Baringo, "A stochastic adaptive robust optimization approach for the offering strategy of a virtual power plant," *IEEE Transactions on Power Systems*, vol. 32, no. 5, pp. 3492–3504, 2016.
[32] T. P. Chang, "Estimation of wind energy potential using different probability density functions," *Applied Energy*, vol. 88, no. 5, pp. 1848–1856, 2011.